

# Influence of residual stresses on fatigue strength of large-scale welded assembly joints

Jakob Klassen<sup>1</sup> · Nils Friedrich<sup>2</sup> · Wolfgang Fricke<sup>2</sup> · Thomas Nitschke-Pagel<sup>1</sup> · Klaus Dilger<sup>1</sup>

Received: 5 August 2016 / Accepted: 28 November 2016 / Published online: 19 December 2016  
© International Institute of Welding 2016

**Abstract** Residual stresses (RS) are known to affect fatigue strength of welded structures in some way. The amount of these residual stresses depends on heat input, the volume of the weld deposit, the number of passes in each weld, and the number of adjacent welds. Therefore, residual stress states are of interest in the design state already. However, determination possibilities by measuring are limited and costly. Numerical welding simulation might be helpful. However, numerical welding simulation still is a challenging task, especially in large-scale modeling and multi-pass welding, calling for simplified methods and models. Even if one is able to calculate residual stresses, their effect on fatigue strength of large-scale welded structures remains uncertain. During fatigue assessment, it is often assumed that tensile residual stresses up to yield strength of the material are present. On the other hand, it is known that residual stresses are redistributed during cyclic loading, thus reducing their effect on fatigue. In this work, experimental and numerical investigations on large-scale components are presented. Fatigue tests were performed and residual stresses (X-ray) were determined at different states, before and during cyclic loading. Calculated and measured results are compared. The influence of residual stresses on

fatigue strength with respect to cyclic redistribution is discussed. This paper represents some of the most meaningful results of a recently finished research project. Further information and results in more detail of this work can be found in the report of Dilger et al. (AiF-Schlussbericht, IGF-Vorhabensnummer 17652N, 2016).

**Keywords (IIW Thesaurus)** Residual stresses · Simulating · Finite element analysis · Fatigue strength · MAG welding

## 1 Introduction

It is well-known that residual stresses may affect the strength of welded structures, in particular the fatigue strength of cyclically loaded components. Residual stresses are mainly induced by the welding process. Reasons for their generation are mainly the shrinkage restraint by the surrounding colder material, phase transformations during cooling, and global structural constraints [1]. Also, the amount of heat input, the volume of the weld deposit, and the number of passes play a role.

Residual stresses can be determined experimentally and numerically. Several experimental methods exist [2] which can be subdivided into destructive and non-destructive methods. The most popular destructive method is bore-hole drilling which can yield a stress profile over the depth of the hole. Non-destructive methods frequently make use of the lattice deformation of the material during straining, for instance, the X-ray diffraction method being able to analyze the residual stresses close to the structural surface. Other methods like the neutron diffraction method allow measurements within the material; however, the effort and costs are much higher.

---

Recommended for publication by Commission XIII - Fatigue of Welded Components and Structures

---

✉ Jakob Klassen  
j.klassen@tu-braunschweig.de

<sup>1</sup> Institute of Joining and Welding, Technische Universität Braunschweig, Braunschweig, Germany

<sup>2</sup> Institute for Ship Structural Design and Analysis, Hamburg University of Technology, Hamburg, Germany

The increasing power of computers and numerical methods such as the finite element method offer possibilities to calculate welding-induced residual stresses numerically [1, 3]. The first step is the analysis of the temperature field due to a moving heat source which was formulated already decades ago [4, 5]. Different phenomena such as the formation of the arc with plasma flux, the vaporization at the surface of the molten weld pool, the melting and dropping of the electrode, and the forming of the weld bead surface were increasingly included in the investigations [6–10]. Up to then, the individual models were only partially combined to models for engineering purposes [11]. Further development of the welding simulation techniques allowed the numerical analysis of the temperature field and the elastic-plastic response of the material with refined finite element models considering realistic heat sources, temperature-dependent material properties, and special effects such as phase transformation [3, 12, 13]. However, several uncertainties still exist, causing large variations if results from different analyses are compared [14]. Furthermore, the computational effort is still very large if longer welded joints or larger structures are investigated [15], calling for simplified methods and models.

The question to what extent residual stresses affect the fatigue strength of welded structures is of practical importance. It is frequently assumed that residual stresses may act in a similar way as mean stresses so that they can approximately be superimposed to mean stresses. In fatigue assessment approaches, it is often assumed that high tensile residual stresses are present. Finally, it is expected that the sum of residual stresses and mean stresses will reach the yield strength of the material [16]. On the other hand, when applying significant load levels, high local residual stresses are relaxed during the first loading cycles [17], reducing their effect on fatigue. This has been observed particularly for local residual stresses adjacent to the weld. Residual stresses due to global structural constraints, sometimes also termed reaction stresses, have found to be more stable [15] so that their effect on fatigue strength can be higher, which has also been observed during testing of larger components [18].

Recently performed tests of large-scale structures concerned web frame corners typical in shipbuilding containing an assembly joint [19]. The first fatigue cracks did not occur at the most highly stressed cruciform joint, but at the fillet weld around the cutout arranged for proper welding. It was suspected that tensile residual stresses were responsible for this unexpected result, leading to the first crack at a hot spot with smaller load-induced stresses. Questions about the criticality of residual stresses at such assembly joints initiated a research project where residual stresses in large-scale models induced by welding of the assembly joint and probably relaxed by the first load cycles are measured and computed. Also, the scale of the models was varied. The principal results of this project are presented in the following.

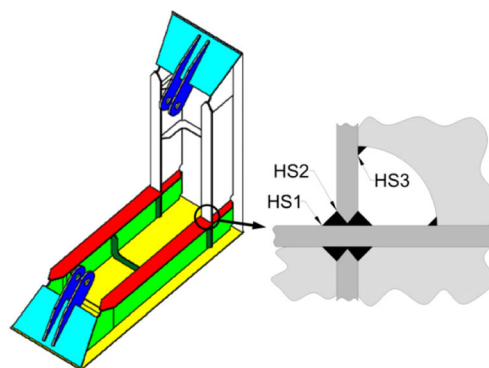


Fig. 1 Web frame corner and critical hot spots (HS) [19]

## 2 Test specimens

### 2.1 Geometry

For the experimental tests, a web frame corner common in many steel and ship structures was chosen. In a previous study [19], fatigue tests on this structural detail (shown in Fig. 1) resulted in uncertainties about the influence of residual stresses on the crack initiation at different critical locations. Cracks formed at the weld slot around the cruciform joint (HS3) and at the cruciform joint itself (HS2), with the latter crack being dominant and leading to the rupture of the flange.

In order to investigate the residual stresses, the structure was modified to allow measurements by X-ray diffraction at both critical weld toes. The resulting geometry is represented in Figs. 2 and 3 with the critical weld at the weld slot (HS3) transferred to the outside of the flange at the end of a longitudinal stiffener. Two different model scales were investigated: full-scale as in ship structures (flange thickness:  $t = 20$  mm) and scaled-down 1:2. A total of eight full-scale and 12 scaled models were used for the tests.

### 2.2 Material properties

The material used was A36 shipbuilding steel with a nominal yield strength of 355 MPa. Additionally, one full-scale model was made of S460. The actual strength values from tension tests were higher than the nominal ones, as shown in Fig. 4. The chemical composition of the employed steels is given in Table 1.

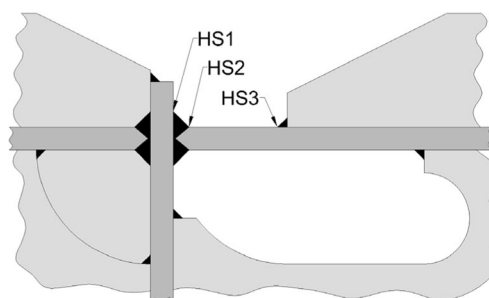
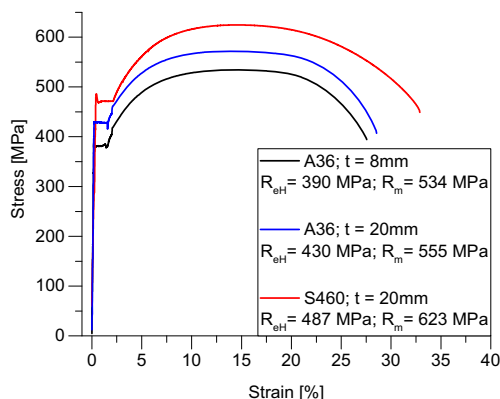
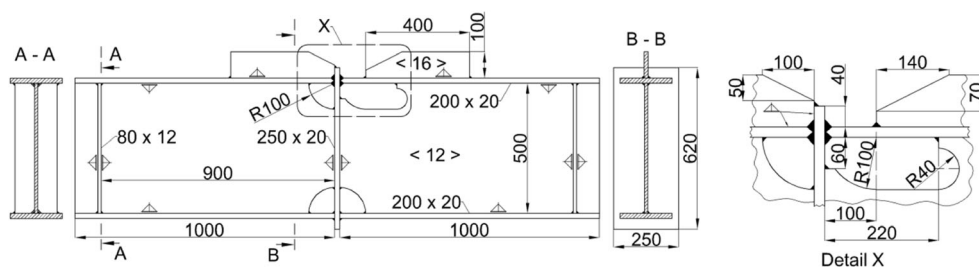


Fig. 2 HS3 transferred to the outside of the flange

**Fig. 3** Dimensions of the full-scale samples



**Fig. 4** Experimentally obtained stress-strain curves

**2.3 Weld sequence**

All specimens were welded using the MAG process. For both scales, the left half component including the vertical flange and the right half component were pre-assembled on two different ship yards; each was responsible for one scale. Then, the longitudinal stiffener on the right side and the assembly joint were welded in the sequence 1–5, as shown in Fig. 5. Meanwhile, welding temperatures near the weld were measured by thermocouples as these data were used to calibrate the numerical models. The cutouts for welding, e.g., no. 4 in Fig. 5, were closed by inserted plates to avoid possible cracks.

The cruciform joints (HS2) in both scales were welded in the same sequence resulting in different numbers of layers (Fig. 6). For the full-scale models, the number of layers varied further due to different gap sizes.

To investigate the influence of residual stresses on fatigue strength, part of the models was stress-relief heat-treated after

welding the assembly joint. Additionally, to reduce the influence of the residual stresses induced by preprocessing, one model of each scale was stress-relieved already after pre-assembly, i.e., before welding the longitudinal stiffener (no. 1 in Fig. 5). An overview of the investigated samples is given in Table 2.

**3 Residual stresses**

**3.1 Residual stress measurement**

Near-surface residual stresses were measured by means of X-ray diffraction (XRD). An evaluation path was the same for both scales and finite element analyses, one line from the longitudinal stiffener to the cruciform joint (Fig. 7). Measurements were performed at each processing state, which were after delivering prefabricated components, after assembly joints were produced, and after a predefined number of load cycles were applied. The latter measurement was done to evaluate residual stress redistribution during fatigue testing.

In as-delivered condition, compressive residual stresses near the surface were found from –250 to –350 MPa at maximum depending on the manufacturer. Assigned longitudinal residual stresses are in welding direction of the cruciform joint. Residual stresses in transverse direction were measured and evaluated in numerical models perpendicular to the cruciform joint between the two weld toes, the cruciform joint (CJ) and longitudinal stiffener (LS) (Fig. 7).

Test components were investigated in three different states for both scales:

1. Pre-heat-treated condition: prefabricated parts were stress-relief heat-treated before welding the assembly

**Table 1** Chemical compositions by weight [%] according to chemical analysis

Steel	Percent by weight [%]									
	C	Si	Mn	P	S	V	Al	Ti	Cr	Ni
A36 (1:2 specimens)	0.16	0.21	1.45	0.021	0.002	0.003	0.038	0.016	0.12	0.064
A36 (1:1)	0.15	0.35	1.42	0.018	0.005	0.002	0.029	0.018	0.03	0.020
S460 (1:1)	0.14	0.33	1.52	0.012	0.002	0.160	0.016	0.001	0.09	0.510

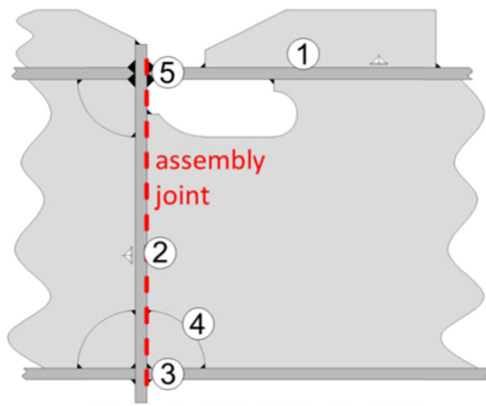


**Fig. 5** Weld sequence of longitudinal stiffener (1) and assembly joint (2–5)

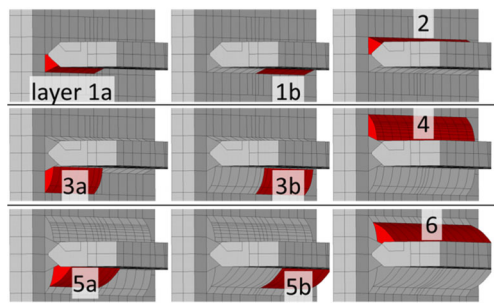


**Fig. 6** Weld sequence at the cruciform joint, further layers on full-scale models

**Table 2** Tested samples

Condition	Full-scale	1:2 scaled
As-welded	4	6
Stress-relieved	3	5
Pre-heat-treated	1	1

joint was carried out. Thus, influences of previous manufacturing steps on residual stress states were eliminated. This state is particularly important for comparison with numerical simulations.

2. Stress-relief heat-treated condition (after welding the assembly joints).
3. As-welded condition: no heat treatment at all, neither before nor after welding.

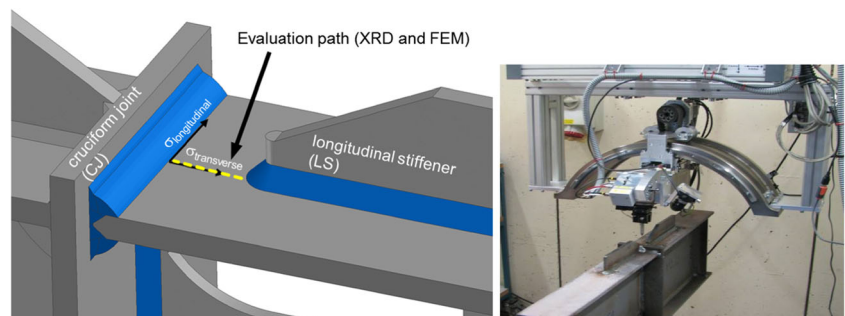
In the following, results of different states are shown for large-scale and 1:2-scaled components. In each case in Fig. 8 through Fig. 10, residual stress distribution is shown on the left hand side and the corresponding weld buildup on the right. In both measuring directions, different residual stresses were found for different preprocessing states (compare M4 with M1 and M3). However, residual stresses for similar preprocessing states (Figs. 9 and 10) were found to be comparable, even though weld buildup varied. The same tendencies were found for scaled components.

Stress-relief heat treatment after welding the assembly joints was carried out successfully, as the results of residual stress measurements in Fig. 11 were revealed. Furthermore, comparison of residual stresses in pre-heat-treated and as-welded condition is shown in Fig. 12. Residual stresses near the heat-affected weld toes are of the same amount and sign. However, the areas between weld toes showed compressive residual stresses. This is due to blast cleaning processes on ship yards. This residual stress pre-state has to be kept in mind when comparing calculated with measured residual stresses.

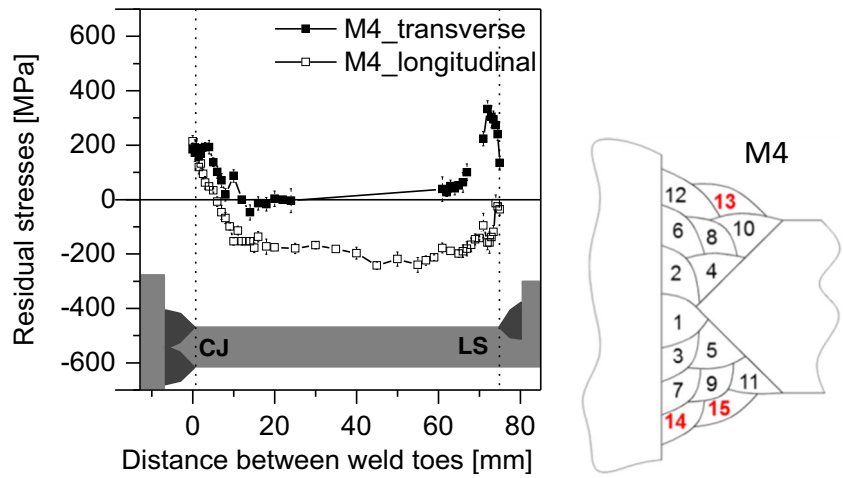
One major focus of this research project was to evaluate possible scalability. The idea was to calculate residual stresses using smaller and less time-consuming FE models. The results were compared with those of large-scale models. Unfortunately, residual stresses were not entirely comparable already through measurements, as can be seen in Fig. 13.

These results reveal that residual stresses around the weld toe of the cruciform joints were quite comparable. However, weld toe regions of the end faces of longitudinal stiffeners were different by means of amount and sign, especially in a transverse direction. Reasons for this are seen in different weld buildups of stiffener end faces. Large-scale components had twice the plate thickness. Therefore, chamfers had to be

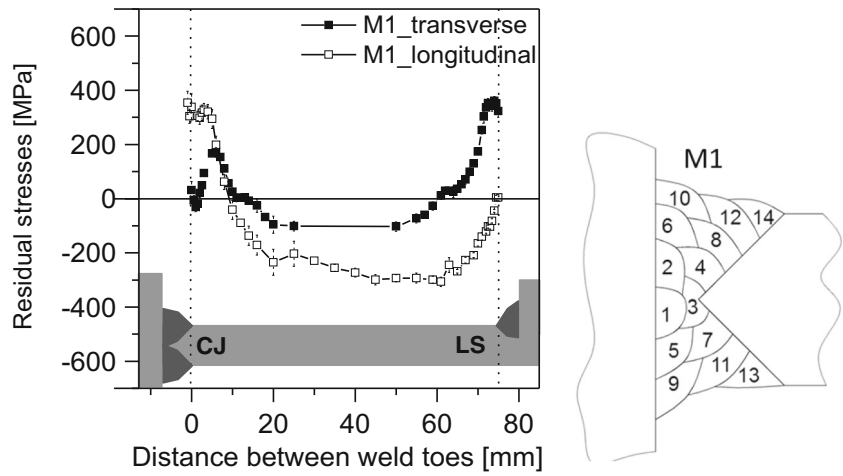
**Fig. 7** Direction of measured and evaluated residual stresses for all specimens with evaluation path for XRD and FEM (left) and exemplary presentation of XRD measurement (right)



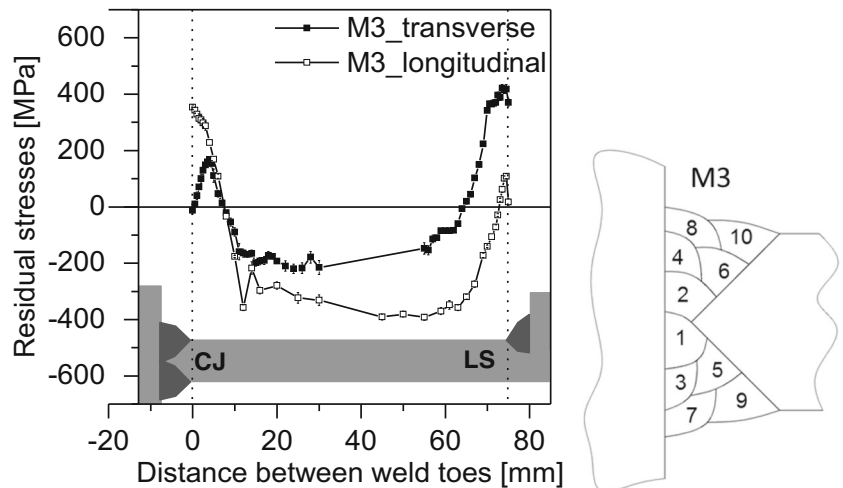
**Fig. 8** Residual stresses in specimen M4 (scale 1:1; heat-treated before welding (*left*)). Corresponding weld buildup (*right*)



**Fig. 9** Residual stresses in specimen M1 (scale 1:1; as-welded (*left*)). Corresponding weld buildup (*right*)



**Fig. 10** Residual stresses in specimen M3 (scale 1:1; as-welded (*left*)). Corresponding weld buildup (*right*)





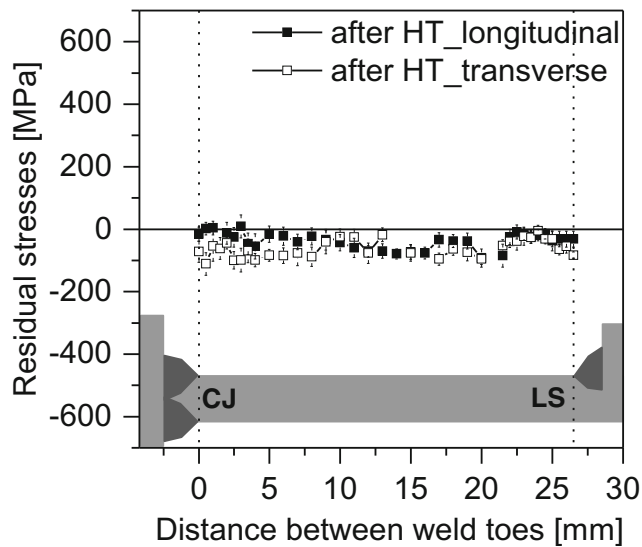


**Fig. 11** Residual stresses after welding and stress-relief heat treatment (HT after assembly joint)

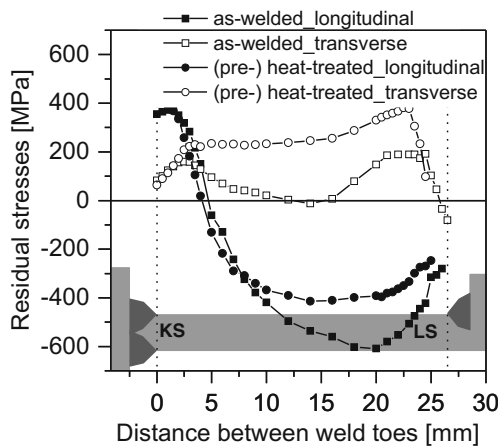


**Fig. 12** Comparison of residual stresses in pre-heat-treated and as-welded condition (mean values of four components)

**Fig. 13** Comparison of residual stresses in specimens of both scales in as-welded condition, longitudinal residual stresses (left) and transverse residual stresses (right)

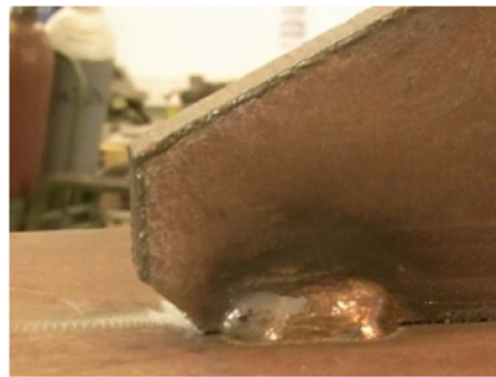
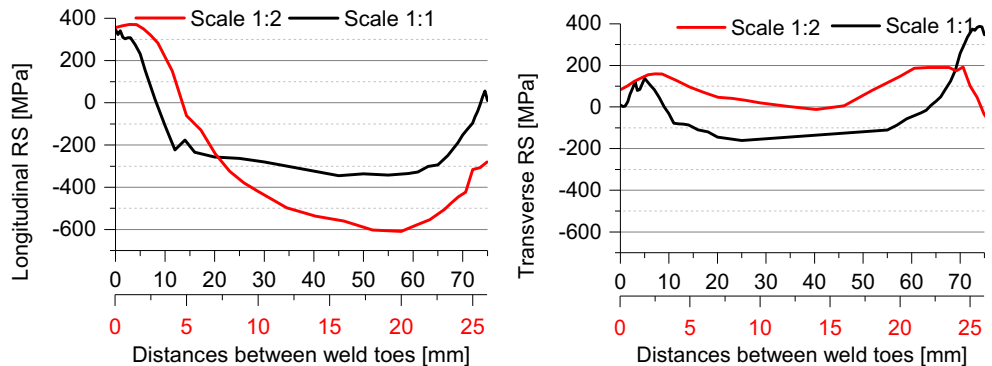


**Fig. 14** Weld detail—end face of a longitudinal stiffener, scale 1:1

applied in weld preparation (compare Fig. 14). As a result of this, weld buildup in large-scale components corresponded to short fillet welds rather than to semicircle welding (Fig. 15). The latter has to be welded with significantly higher welding speed, thus resulting in higher cooling rates and different residual stress states near the weld toe.

### 3.2 Residual stress redistribution due to cyclic loading

Residual stress state redistribution during fatigue testing was determined by measuring the same components after a predefined number of load cycles. Both scale components were measured after  $N = 0$ ,  $N = 1$ , and  $N = 10$  (and  $N = 10,000$  for one 1:2-scaled component) load cycles. Results are shown in Fig. 16 for scale 1:1. Figures 17 and 18 show measuring results for two different components scaled 1:2.

Although scaling in diagrams is unchanged for clarity and comparability reasons, residual stress redistribution still is apparent, especially in the weld toe region of the longitudinal stiffener. Furthermore, it can be stated that residual stress redistribution is almost stable after the first load cycle. As can be seen in Fig. 17, residual stress states after the first load cycle do not differ from the state after 10,000 cycles. This result applied to components of both scales.

It can be found in literature that when applying pulsating tensile stress, welding residual stresses should have a

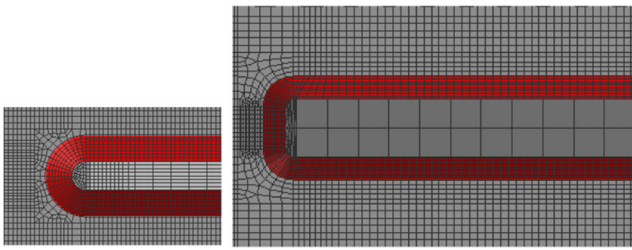


**Fig. 15** Comparison of modeled weld beads in different scale FE models, true to scale

negligible effect on cyclically loaded specimens with welded longitudinal stiffeners, e.g., [18, 20] or [21]. The reason for this is a stabilized residual stress redistribution after the first load cycles. Furthermore, sharp notch radius will reduce the mean stress influence. On the other hand, it can also be found in literature that welding residual stresses should have an influence on fatigue of cruciform joints, as stated in [22]. However, these results are based on small-scale specimens and just one weld detail in each case. But there still is a lack

**Fig. 16** Residual stress redistribution from cyclic loading (scale 1:1, as-welded, specimen M3). Transverse direction (left) and longitudinal direction (right)

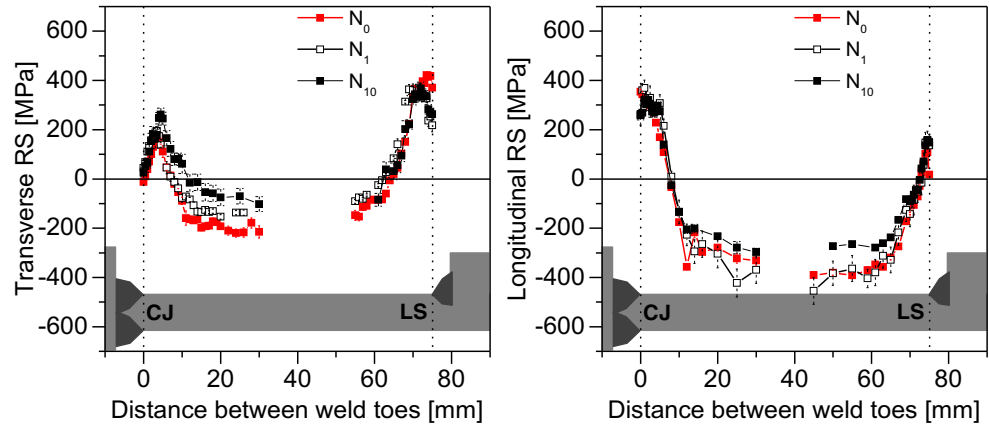


**Fig. 17** Residual stress redistribution from cyclic loading (scale 1:2, as-welded, specimen M2). Transverse direction (left), longitudinal direction (right)

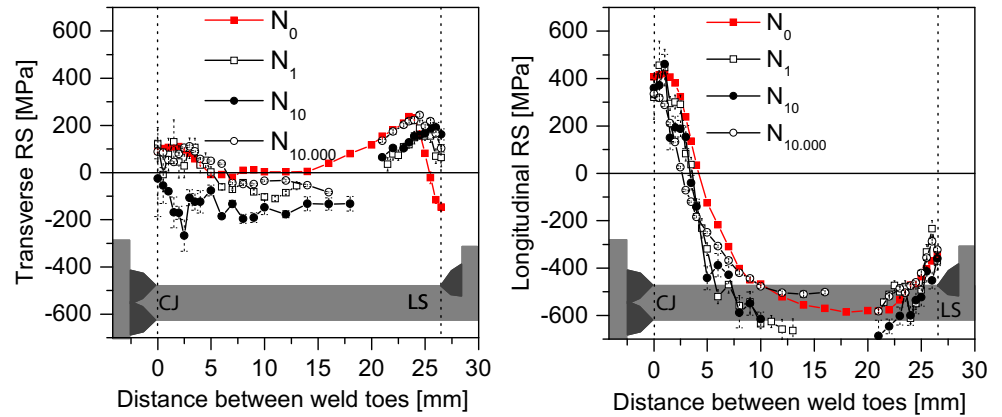
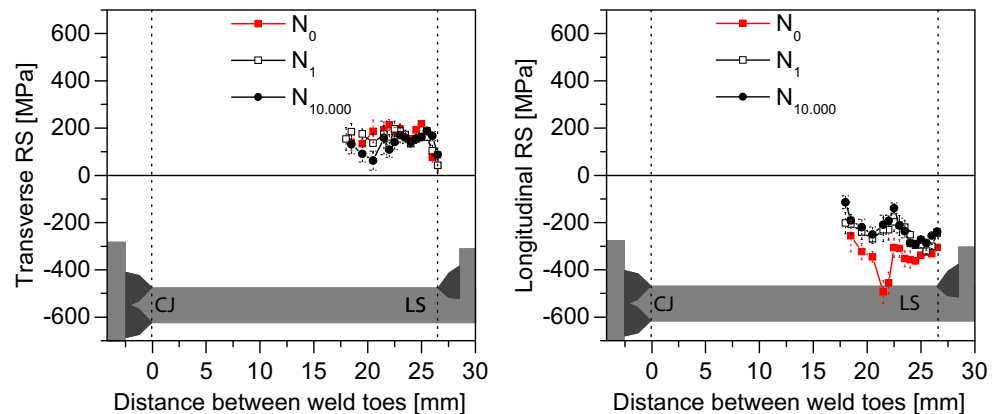


**Fig. 18** Residual stress redistribution from cyclic loading (scale 1:2, as-welded, specimen M9). Transverse direction (left), longitudinal direction (right)



of experimental results on larger components with several weld details which are affecting each other.

#### 4 Fatigue testing

Fatigue tests were carried out on components of both scales under pulsating bending in the as-welded and stress-relief heat-treated condition. The tests were performed with a constant load range and a stress ratio of  $R = 0.1$ . These load-induced stresses are superimposed on stabilized residual stress levels. To obtain stabilized residual stress states, repetitive measurements were carried out after a number of load cycles (as described above). Furthermore, the same number of load cycles was used on numerical models to back up experimentally obtained data.

For evaluation of fatigue tests, the structural hot spot stresses were calculated according to [23]. Fatigue tests were accompanied by strain gauges and penetrating tests to find and follow cracking during experiments. Unfortunately, crack initiation areas were not obvious, since the entire component had shown several weld toes and sharp notches. During testing, several crack initiation areas were localized. Because strain gauges were applied between the weld toes of cruciform joints and end faces of longitudinal stiffeners, two different failure criteria were used for evaluating experimental data. The first failure criterion was an assumed crack initiation. This was defined as a decrease of maximum strain by 10% at the gauge closest to the weld. The second criterion was crack penetrating the top flange plate.

##### 4.1 Scale 1:1

The fatigue tests were performed in a three-point bending setup, as shown in Fig. 19. The load was applied by a 1200-

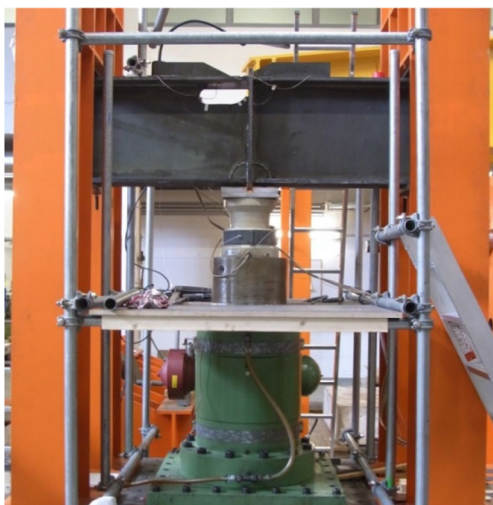


**Fig. 19** Setup for fatigue tests (full-scale)

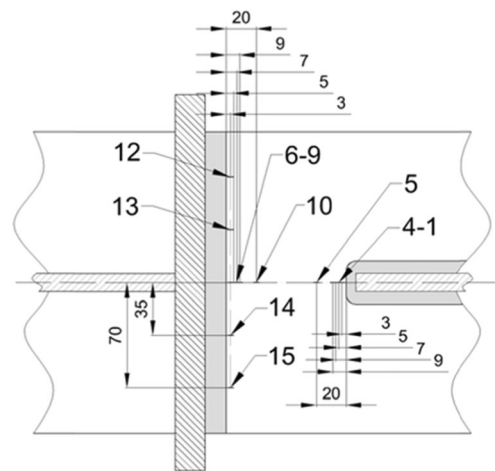


**Fig. 20** Strain gauge arrangement at the cruciform joint and the longitudinal stiffener

kN hydraulic cylinder. The specimens were simply supported at their ends. Strains at the investigated welds were measured by means of strain gauges applied as shown in Fig. 20. Several strain gauges at different distances from the weld toe allowed the extrapolation of structural hot spot stresses to the investigated hot spots. Three different load levels were applied. One stress-relieved and at least one as-welded specimen were tested at each level. The nominal and structural hot spot stress ranges are given in Table 3. Contrary to the original web frame corner, structural hot spot stresses were higher at the longitudinal stiffener (HS3) than at the cruciform joint (HS2).

On all full-scale specimens, the first cracks were detected at the end face of the longitudinal stiffener (HS3). For all specimens (except on two), these cracks led to the failure of the flange ending the fatigue test. On two specimens (M4 and M7), cracks initiated at the cruciform joint (HS2). On these two specimens, additional top layers had been added, possibly

**Table 3** Nominal and structural hot spot stress ranges in full-scale fatigue tests (HS2: cruciform joint; HS3: longitudinal stiffener)

Specimen	Condition	Load range [kN]	Nominal stress range [MPa]		Structural hot spot stress range [MPa]	
			HS2	HS3	HS2	HS3
M1	As-welded	650	118	108	196	212
M2	Stress-relieved	650	118	108	190	209
M3	As-welded	570	103	94	181	185
M4	As-welded <sup>a</sup>	500	91	83	156	180
M5	Stress-relieved	570	103	94	178	194
M6	Stress-relieved	500	91	83	150	154
M7	As-welded	650	118	108	213	228
M8 (S460)	As-welded	570	103	94	173	210

<sup>a</sup> Stress-relieved after pre-assembling and before welding the assembly joint



**Fig. 21** S-N diagram for structural hot spot stress range and the number of load cycles until 10% strain reduction (SR stress-relieved, AW as-welded)

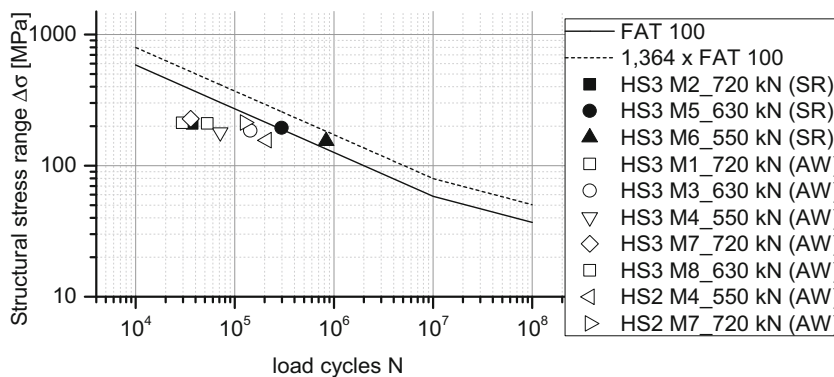
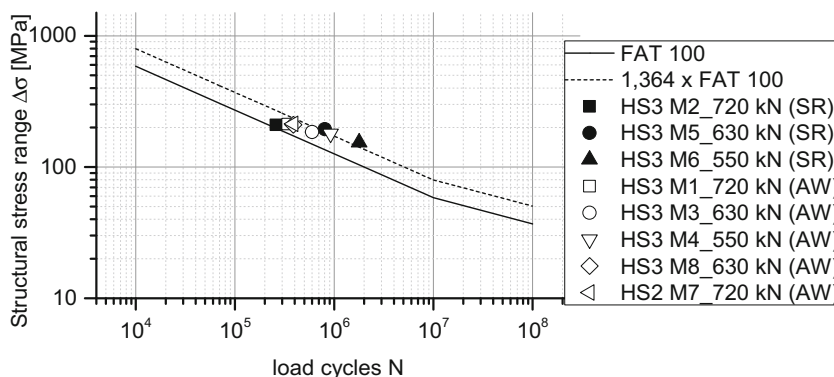


**Fig. 22** S-N diagram for structural hot-spot stress range and the number of load cycles until the crack strikes through the girder (SR stress-relieved, AW as-welded)



causing a higher residual stress level. For one of these specimens, the failure of the flange occurred at the cruciform joint.

To determine crack initiation, the strain in front of the hot spots was evaluated. The S-N diagram for crack initiation defined in this way is shown in Fig. 21. Failure of the specimen was defined by the crack penetrating the flange. The S-N diagram for this failure criterion is shown in Fig. 22.

#### 4.2 Scale 1:2

Experimental setup for fatigue testing of 1:2-scaled components is shown in Fig. 23. Similar strain measuring was



**Fig. 23** Experimental setup for fatigue testing of 1:2-scaled components

applied as for the original scale components. An example of applied strain gauges and penetrating tests for crack growth determination is shown in Fig. 24.

In almost all (except one) 1:2-scaled specimens, the first cracks were detected at weld toes of the longitudinal stiffeners (HS3). These cracks caused strongly increasing strains in the machine control strain gauges and the fatigue tests were ended in this stadium. In one case, a crack initiated at the cruciform joint. However, another crack formed at the weld toe of the stiffener just a few load cycles later. This latter crack, although initiated later, outran the first crack and again was responsible for overall component failure.

As described above, crack initiation was assumed when maximum strain decreased by 10%. The S-N



**Fig. 24** Exemplary picture of applied stress gauges. At weld toe of the longitudinal stiffener (left), stress gauges for machine control on the opposite bottom side with crack highlighted through penetration testing (right)

**Fig. 25** S-N diagram for a structural hot spot stress range and the number of load cycles until the crack penetrates the girder (SR stress-relieved, AW as-welded)

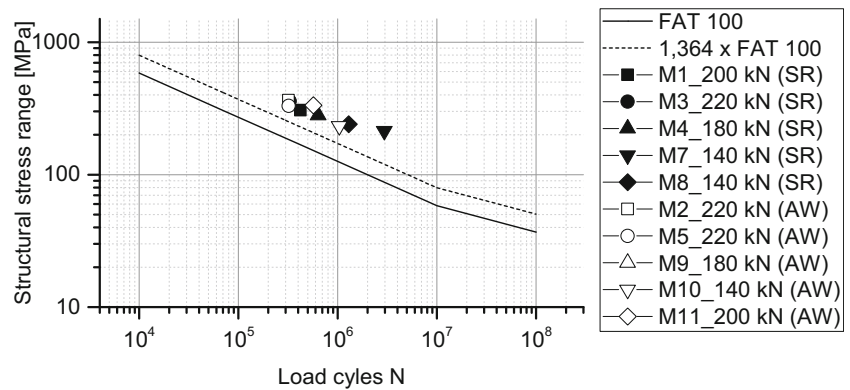
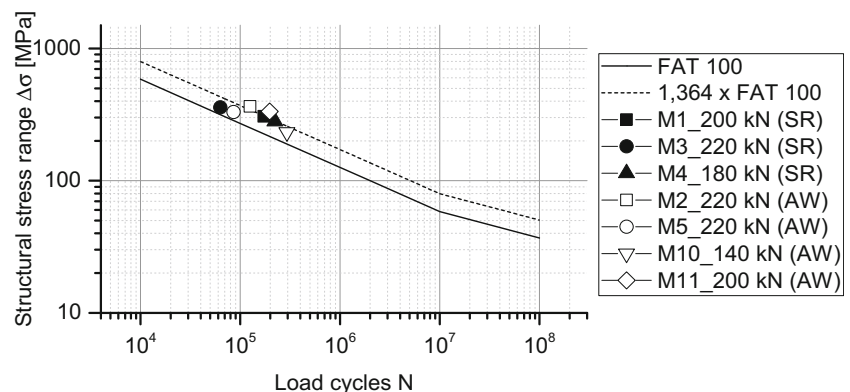


diagram for crack initiation defined in this way is shown in Fig. 25. Failure of the specimen was defined by the crack penetrating the flange. The S-N diagram for this failure criterion is shown in Fig. 26.

## 5 Numerical welding simulation

Numerical welding simulations by means of structural finite element analyses were carried out with two different codes, SYSWELD (Sysweld 2015.1, Version 17) and ANSYS. With the first software phase, transformation has been taken into account by means of using the implemented pre-set parameters for an S355 (material properties are comparable to the used A36 steel grade) of solver code. ANSYS, on the other hand, was considered to determine the influence of phase transformation in numerical welding simulations. To take into account phase transformation using ANSYS, a simplified approach by means of a user subroutine in an in-house code was used. Specimens of both scales were calculated with each software to ensure that there was no software-specific influence on calculated results based on comparable input data. Numerical models were calibrated by measured temperature fields and macrosections of each weld.

**Fig. 26** S-N diagram for a structural hot spot stress range and the number of load cycles until 10% strain reduction (SR stress-relieved, AW as-welded)



### 5.1 Scale 1:1

The simulations of the full-scale models were mostly done in ANSYS. Temperature-dependent material properties were taken for an S355 steel from [24]. The stress-strain curves were scaled to consider the higher yield strength of the specimens. The Von Mises yield criterion and nonlinear isotropic hardening were used to determine the elastic-plastic material behavior.

To reduce computation time, only the investigated section including the cruciform joint and the longitudinal stiffener was modeled with solid elements and the surrounding structure consisted of shell elements as shown in Fig. 27. To transmit the bending moments from shell to solid elements, a layer of shell elements having the thickness of the girder was arranged on the face of the solids over the plate thickness. No relevant differences in the resulting temperatures or stresses have been observed compared to models using only solid elements. The number of weld layers at the cruciform joint has been varied according to the actual specimens; Figure 27 shows a model with 11 layers. The number of elements was approximately 220,000 varying with the number of weld layers at the cruciform joint. The smallest element size in the weld was set to 0.5 mm.

The welding simulations were carried out in two steps. First, a transient thermal analysis was performed in which

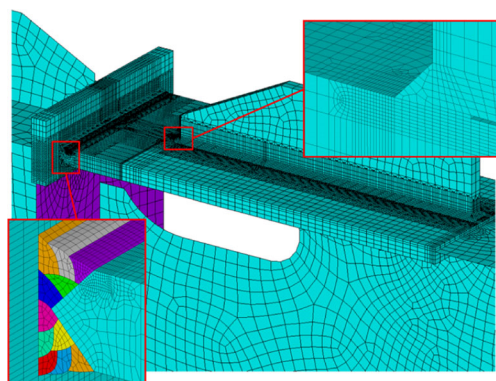


**Fig. 27** An FE model with shell elements and solids in the investigated area around the cruciform joint and the longitudinal stiffener

the welding energy is applied by means of a volumetric heat source as described by Goldak [12]. Typical values for the heat source were 484 J/mm energy input and dimensions of  $12 \times 7 \times 4$  mm ( $L \times W \times D$ ). The parameters varied slightly for the different weld layers. The result was the temperature distribution for each time step. The heat source was calibrated by comparing calculated temperatures near the weld path with the ones measured during the welding of the models as shown in Fig. 28. The extent of the heat source was validated by comparing temperature distributions at the weld zone with the extent of the molten and the heat-affected zone in the macrograph of the weld (Fig. 29).

In a second step, the structural analysis was carried out. The calculated temperature field for each load step was imposed as load, and the deformations and stresses resulting from the heating and cooling of the material were computed.

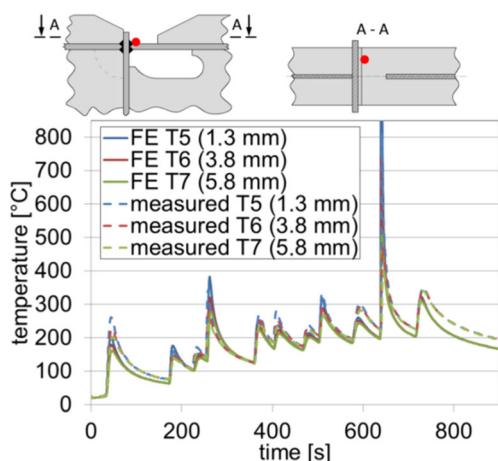


**Fig. 28** Calculated (FE) and measured temperatures (thermocouples T5–7) at the cruciform joint of a full-scale model

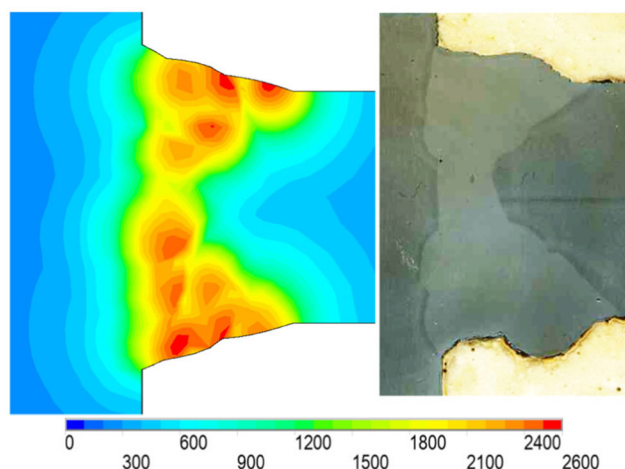


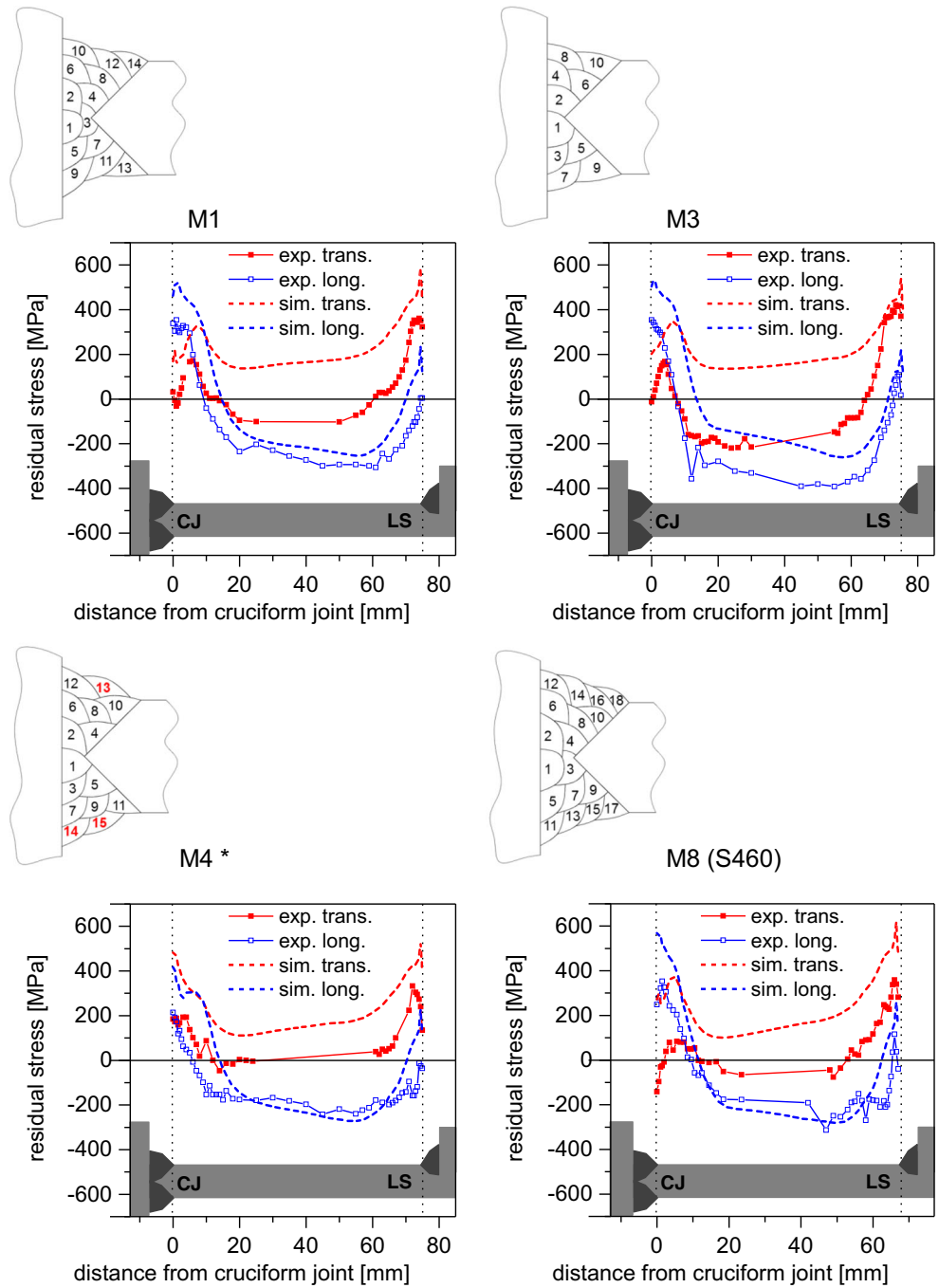
**Fig. 29** Calculated maximum temperatures (°C) reached at each node over all load steps and polished macrograph

The resulting residual stresses, calculated without consideration of phase transformation, are compared with the measurements in Fig. 30. In the center between the cruciform joint and longitudinal stiffener, the results show a considerable difference. This is due to the compressive residual stresses of approximately  $-300$  MPa on the plate surface which were not considered in the simulation. Close to the welds, calculated values are higher than the measurements.

In order to achieve a better agreement with the measured residual stresses, a simplified approach to consider phase transformation effects based on [25] was used. To consider dilatation during the austenite back transformation, a second curve for the thermal expansion used for cooling was implemented as shown in Fig. 31. Material properties were switched to the cooling curve when one node of an element had reached  $900$  °C. Phase transformation was then assumed from  $500$  to  $300$  °C. Phase transformation plasticity (TRIP) was considered by a decreased yield strength during the transformation as shown in Fig. 32.

The residual stresses calculated with this simplified consideration of phase transformation effects are shown in Fig. 33 for the model M3. At the cruciform joint, a better agreement with measurements could be achieved. At the longitudinal stiffener, little difference compared to the simulation without phase transformation was observed. Simulation results for the other models showed a similar improvement compared to the corresponding measurements. For the model M3 also, a welding simulation in SYSWELD including phase transformation was done. The results are shown in Fig. 34. The calculated residual stresses are similar to those from the simulation with the simplified phase transformation in Fig. 33.

**Fig. 30** Calculated and measured residual stresses for models with different numbers of layers at the cruciform joint



\*) stress-relieved after preassembling, before welding the assembly joint

**5.2 Scale 1:2**

A numerical model with FE mesh of the 1:2-scaled component is shown in Fig. 35. The calculated weld beads are highlighted in red. Comparison of calculated and measured residual stresses are shown in Fig. 36 for the scaled model.

As this figure shows, the results correspond well with each other. Especially, residual stresses near the end-face weld toe of the longitudinal stiffener were calculated rather accurately. This area was found to be most important, since most components broke here in fatigue testing.



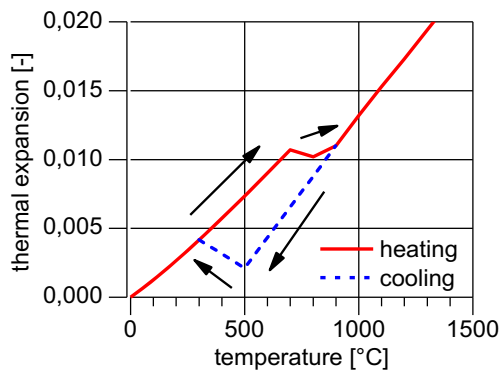


**Fig. 31** Thermal expansion with phase transformation between 500 and 300 °C

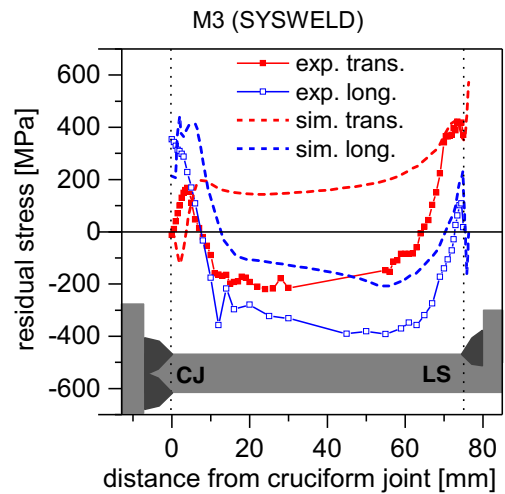


**Fig. 34** Residual stresses calculated with SYSWELD including phase transformation compared with measurements

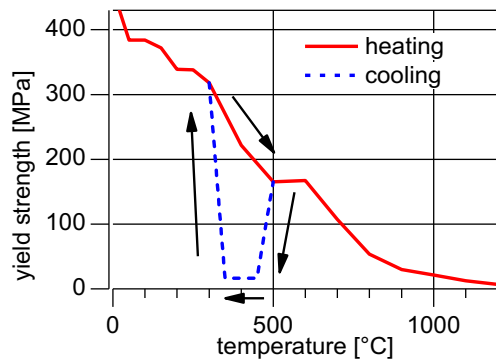


**Fig. 32** Reduced yield strength to consider transformation-induced plasticity (TRIP)

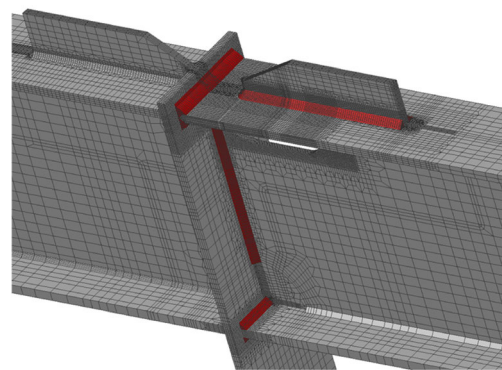


**Fig. 35** A numerical model of scaled specimen. Calculated weld beads in red

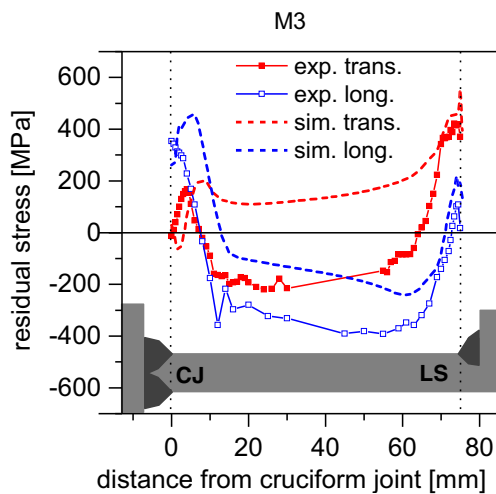


**Fig. 33** Calculated residual stresses with a simplified consideration of phase transformation effects compared with measurements

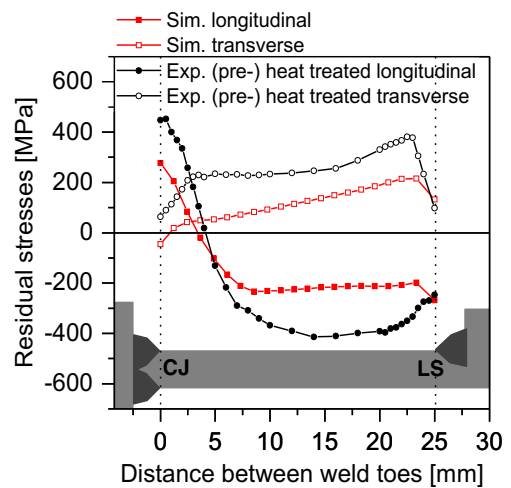


**Fig. 36** Comparison between calculated and measured residual stresses in pre-heat-treated condition, scale 1:2



## 6 Conclusions

Experimental and numerical investigations on the influence of residual stresses on fatigue strength of welded assembly joints have been performed. Tested components represented a web frame corner, which is typical in ship structures. These specimens included two typical weld geometries, the cruciform joint and longitudinal stiffener. Specimens in two scales have been tested. Residual stresses have been measured by means of X-ray diffraction. At the cruciform joint, the measurements yielded comparable results although the number of weld layers varied. At the longitudinal stiffener, results differed between the two scales due to the different plate thicknesses which affected cooling rates and the geometry of the welds. Repeated measurements after cyclic loading showed that residual stress redistribution took place during the first load cycle.

Fatigue tests have been carried out in as-welded and stress-relief heat-treated conditions. The results showed no clear residual stress influence on the fatigue life of the investigated welds. Residual stresses might have affected the crack initiation at both the cruciform joint and longitudinal stiffener. However, stress concentration in the weld toes of longitudinal stiffeners was rather high and thus responsible for component failure.

Numerical welding simulations have been performed. Comparison between calculated and measured residual stresses showed good agreement, provided that phase transformation effects were taken into account. Due to compressive residual stresses caused by manufacturing of the sheets (not taken into account in simulations), the values showed larger differences at the center of the plate not directly affected by the heat of the welds. The assumption of isotropic hardening may have caused an overestimation of residual stresses at the weld.

**Acknowledgements** We would like to thank the German Federation of Industrial Research Associations (AiF) for its financial support of the research project IGF-Nr. 17652N. This project was carried out under the auspices of the AiF and financed within the budget of the German Federal Ministry of Economics and Technology (BMWi) through the program to promote joint industrial research and development (IGF). Special thanks to the EDL Ems Dienstleistung GmbH and the Meyer Werft GmbH & Co. KG as well as the Flensburger Schiffbau-Gesellschaft mbH & Co. KG for carrying out the welding work and the preparation of components.

## References

- Radaj D (2003) Welding residual stresses and distortion. DVS-Verlag, Düsseldorf
- Kandil FA, Lord JD, Fry AT, Grant P (2001) A review of residual stress measurement methods—a guide to technique selection. National Physics Laboratory, Teddington Middlesex
- Lindgren L-E (2001) Finite element modeling and simulation of welding part I: increasing complexity, part II: improved material modelling. *J Therm Stresses* 24:141–192 195–231
- Rosenthal D (1946) The theory of moving sources of heat and its application to metal treatments. *Trans ASME*
- Rykalin NN (1957) Berechnung der Wärmevergänge beim Schweißen. VEB Verlag Technik, Berlin
- Karlsson L and Lindgren L (1990) Combined heat and stress-strain calculations. Modeling of casting, welding and advanced solidification processes V: 5th International conference on modeling of casting and welding processes, pp. 187–202
- Lowke JJ, Kovitya P, Schmidt H (1992) Theory of free-burning arc columns including the influence of the cathode. *Journal of Physics D Applied Physics* 25(11):1600–1606
- Choo RT, Szekely J (1994) The possible role of turbulence in GTA weld pool behavior. *Welding Journal Research Supplement* 74(2): 25s–31s
- Ruyter E (1993) Development and assessment of welding procedures for avoiding weld joint cracking in highly restrained offshore steel structures. Hamburg
- Böllinghaus T (1995) Determination of crack-critical shrinkage restraints and hydrogen distribution in welded joints by numerical simulation (in German). Hamburg
- Dilthey U, Habedank G, Reichel T, Sudnik W, Ivanov A, Mokrov O (1995) MAGSIM program software for analysis, optimisation and diagnostics of the process of consumable electrode welding thin sheet joints in an active gas. *Weld Int* 9:891–896
- Goldak J, Chakravarti A, Bibby M (1984) A new finite element model for welding heat sources. *Metall Trans B* 15:299–305
- Lindgren L-E (2007) Computational welding mechanics—thermomechanical and microstructural simulations. Woodhead Publishing in Materials, Cambridge
- Janosch J (2003) Round robin phase II—first 3D modelling results. IIW-Doc. X-1141-03/XIII-1978-03/XV-1541-03
- Fricke W, Zacke S (2014) Application of welding simulation to block joints in shipbuilding and assessment of welding-induced residual stresses and distortions. *International Journal of Naval Architecture and Ocean Engineering* 6:459–470
- Maddox S (1991) Fatigue strength of welded structures. Abington Publishing, Cambridge
- Farajian M (2010) Stability and relaxation of welding residual stresses. Dissertation, Braunschweig
- Buxbaum O (1986) Betriebsfestigkeit-Sichere und wirtschaftliche Bemessung schwingbruchgefährdeter Bauteile (Fatigue strength - safe and economic design of fatigue-prone components, in German). Verlag Stahleisen mbJ, Düsseldorf
- Fricke W, von Lilienfeld-Toal A, Paetzold H (2012) Fatigue strength investigations of welded details of stiffened plate structures in steel ships. *Int J Fatigue* 34(1):17–26
- Baumgartner J, Bruder T (2013) Influence of weld geometry and residual stresses on the fatigue strength of longitudinal stiffeners. *Welding in the World* 57:841–855
- Yuan K and Sumi Y (2013) Welding residual stress and its effect on fatigue crack propagation after overloading. *Anal Des Mar Struct*
- Krebs J, Kaßner M (2007) Influence of welding residual stresses on fatigue design of welded joints and components. *Welding in the World* 51(7):54–68
- Hobbacher A (2009) Recommendations for fatigue design of welded joints and components. IIW-Doc. 1823–07. *Int Inst Weld*
- Wichers M (2006) Schweißen unter einachsiger, zyklischer Beanspruchung. Experimentelle und numerische Untersuchungen (Welding under uniaxial cyclic loading - experimental and numerical research, in German). Dissertation TU-Braunschweig
- Dilger K, Welters T (2006) Schlussbericht zum BMBF-Verbundprojekt SST-Schweißsimulationstool (report to the BMBF-project SST—welding simulation tool, in German). Shaker Verlag, Aachen